CELL BIOLOGY

The HIPK2/CDC14B-MeCP2 axis enhances the spindle assembly checkpoint block by promoting cyclin B translation

Patrick Partscht[1,2], Alexander Simon[2,3], Nan-Peng Chen[1]†, Sylvia Erhardt[3], Elmar Schiebel[1]*

Mitotic perturbations activate the spindle assembly checkpoint (SAC) that keeps cells in prometaphase with high CDK1 activity. Prolonged mitotic arrest is eventually bypassed by gradual cyclin B decline followed by slippage of cells into G_1 without chromosome segregation, a process that promotes cell transformation and drug resistance. Hitherto, the cyclin B1 decay is exclusively defined by mechanisms that involve its proteasomal degradation. Here, we report that hyperphosphorylated HIPK2 kinase accumulates in mitotic cells and phosphorylates the Rett syndrome protein MeCP2 at Ser^{92}, a regulation that is counteracted by CDC14B phosphatase. $MeCP2^{S92}$ phosphorylation leads to the enhanced translation of cyclin B1, which is important for cells with persistent SAC activation to counteract the proteolytic decline of cyclin B1 and therefore to suspend mitotic slippage. Hence, the HIPK2/CDC14B-MeCP2 axis functions as an enhancer of the SAC-induced mitotic block. Collectively, our study revises the prevailing view of how cells confer a sustainable SAC.

INTRODUCTION

Chemotherapeutic drugs that target the mitotic spindle benefit from the high proliferation rate of tumor cells. Treatment of cells with drugs such as nocodazole (NOC) and paclitaxel or the Eg5 kinesin motor inhibitor STLC (*S*-trityl-L-cysteine) leads to improper or failed binding of kinetochores to spindle microtubules, which, in turn, keeps the spindle assembly checkpoint (SAC) active. The SAC delays mitotic progression by preventing the activation of the anaphase-promoting complex/cyclosome (APC/C) holding eukaryotic cells in prometaphase of mitosis for 12 to 48 hours (*1*, *2*). Prolonged mitosis can lead to apoptosis; however, cells can overcome mitotic arrest by a phenomenon termed mitotic slippage. Mitotic slippage is proposed to limit the effectiveness of chemotherapies using antimitotics; however, how cancer cells are killed by antimitotic chemotherapies is contentiously discussed (*3*, *4*). Cells that undergo slippage exit mitosis without cell division and return to interphase as 4 N-pseudo G_1 cells thereby escaping mitotic cell death and contributing to oncogenesis by inducing tetraploidy with subsequent genomic instability, potentially leading to cell transformation (*5*). Slow degradation of cyclin B1 in the presence of an active SAC is believed to trigger slippage (*6*).

The founding member of CDC14 phosphatases, *Saccharomyces cerevisiae* Cdc14 (ScCdc14), counteracts phosphorylation of mitotic cyclin-dependent kinase 1 (CDK1) and promotes proteolysis of the mitotic cyclin Clb2, thereby resetting CDK1 phosphorylations and enabling mitotic exit (*7*–*10*). In mammalian cells, this CDK1-reversing function is fulfilled by the PP1 (protein phosphatase 1) and PP2 phosphatases (*11*) suggesting that CDC14A and CDC14B have different functions (*12*, *13*). CDC14A mainly regulates the actin cytoskeleton (*14*, *15*), while the role of CDC14B is largely unknown.

Here, we identify the methyl-CpG–binding protein 2 (MeCP2), a chromatin binding protein with functions in brain development, whose malfunction is causing Rett syndrome (*16*), as a CDC14B substrate. We demonstrate counteracting activities on MeCP2 phosphoregulation at ser^{92} by the stress-induced kinase HIPK2 (homeodomain-interacting protein kinase 2) and CDC14B. Mitotic phosphorylation of MeCP2 causes increased translation of cyclin B1 and thus prolonged duration of mitotic arrest due to an increase in CDK1 activity. Inactivation of mitotic MeCP2 phosphorylation promotes mitotic slippage of cells with mitotic defects. Our data indicate that HIPK2-MeCP2 functions as an enhancer of the SAC-imposed mitotic block.

RESULTS

CDC14B dephosphorylates regulators of gene expression

Because the function of CDC14B is largely unknown, we set out to identify CDC14B targets. Substrates of human CDC14B were identified by liquid chromatography–tandem mass spectrometry (LC-MS/MS) comparing the phosphoproteome of HeLa Tet_{ON}-*CDC14B-YFP* and Tet_{ON}-*YFP* cells grown in heavy and light medium, respectively (Fig. 1A). Forty-two proteins including Histone H1x (H1FX), NOC2 Like Nucleolar Associated Transcriptional Repressor (NOC2L), Thyroid Transcription Factor 1 (TTF1), Histone H1.5 (HIST1H1B), Bromodomain Adjacent To Zinc Finger Domain 2A (BAZ2A), and MeCP2 were reproducibly hypophosphorylated upon induction of *CDC14B-YFP* expression compared to the yellow fluorescent protein (YFP) control (Fig. 1, B and C, and table S1). The dephosphorylation events occurred on the pSPxK/R consensus sequence (Fig. 1D) as is the case for ScCdc14 and CDC14A (*7*, *17*, *18*), and Gene Ontology analysis of these hits indicated that CDC14B is involved in the regulation of gene expression (Fig. 1C) consistent with its chromatin association (*12*, *19*). MeCP2 and BAZ2A were confirmed by the proximity-dependent biotin identification (BioID) approach using CDC14B-

[1]Zentrum für Molekulare Biologie, Universität Heidelberg, DKFZ-ZMBH Allianz, Heidelberg 69120, Germany. [2]Heidelberg Biosciences International Graduate School (HBIGS), Universität Heidelberg, Heidelberg, Germany. [3]Zoological Institute, Karlsruhe Institute of Technology (KIT), Karlsruhe 76131, Germany.
†Present address: Max-Planck Institute for Biochemistry, Martinsried 82152, Germany.
*Corresponding author. Email: e.schiebel@zmbh.uni-heidelberg.de

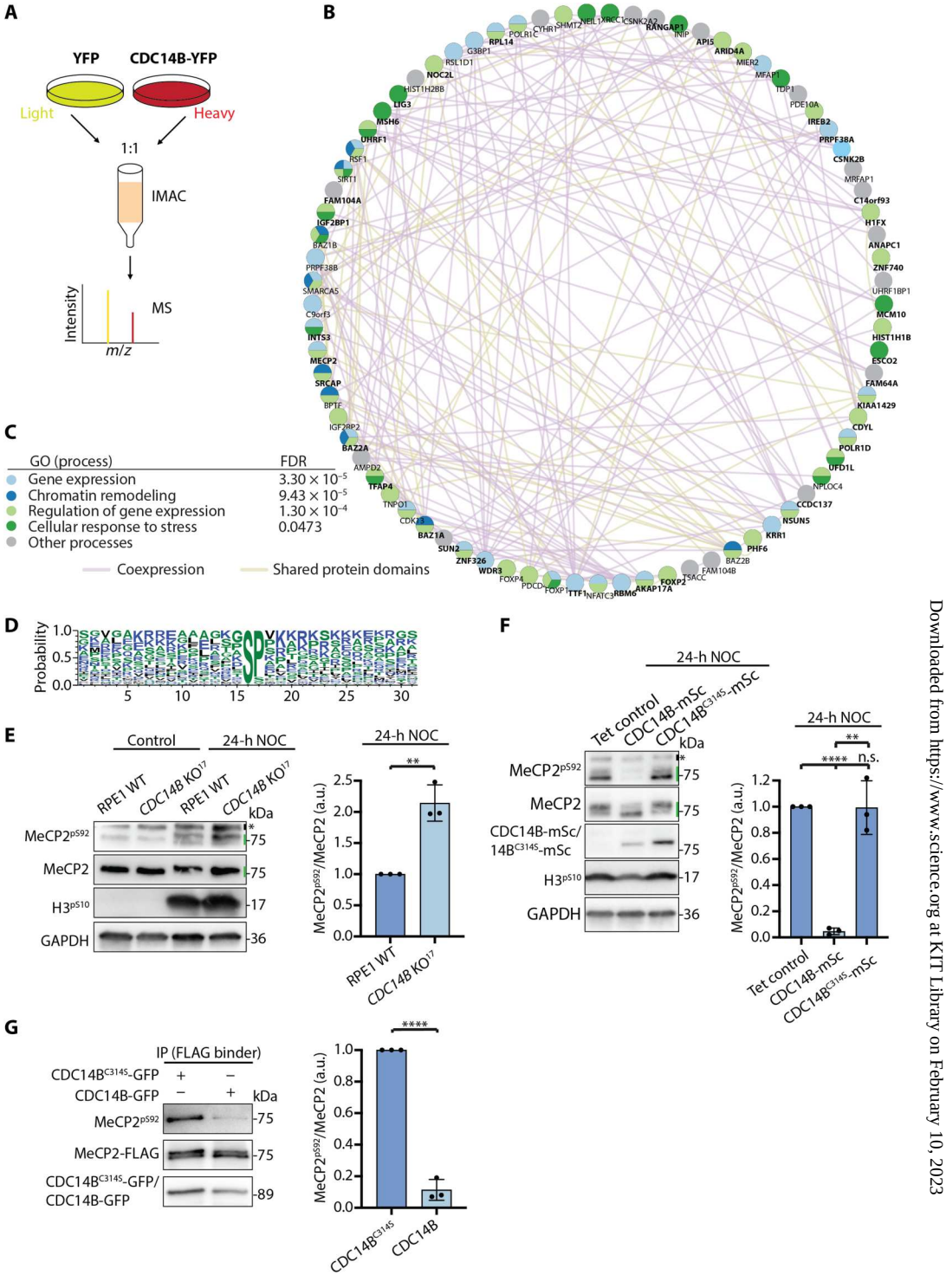

Fig. 1. MeCP2 is a substrate of hCDC14B. (**A**) HeLa *CDC14B-YFP* and HeLa *YFP*-inducible cell lines were grown in heavy and light medium, respectively, to compare the phosphoproteome by mass spectrometry (MS). *m/z*, mass/charge ratio; IMAC, immobilized metal affinity chromatography. (**B**) Molecular network of the hypophosphorylated proteins (hits) from (A). The network was constructed in Cytoscape to extract functional information and shows hits (bold font) and their most related genes (regular font) identified using a guilt-by-association approach. Coexpression and shared protein domains are denoted by purple and yellow lines, respectively. The identified phosphorylation sites are summarized in table S1. (**C**) Gene Ontology (GO) analysis of hypophosphorylated proteins from (B). FDR, false discovery rate. (**D**) Sequence logos of hypophosphorylated p-sites from (A). (**E**) RPE1 WT and RPE1 *CDC14B* KO cells were treated with 3.3 μM NOC for 24 hours to accumulate prometaphase cells with high MeCP2^{pS92} signal. The MeCP2^{pS92}/MeCP2 ratio was densitometrically measured and is depicted in the graph on the right-hand side of the immunoblot. The asterisk indicates nonspecific protein bands that are detected by the anti-MeCP2^{pS92} antibody. Green lines depict position of specific bands. The quantification was performed on three independent experiments. (**F**) RPE1 Tet$_{ON}$ cells expressing *CDC14B-mSc* or the catalytic inactive *CDC14B^{C314S}-mSc* were treated and analyzed as described in (E). Asterisk and lines as in (E). The quantification was performed on three independent experiments. a.u., arbitrary units. (**G**) In vitro dephosphorylation of MeCP2^{pS92} by purified CDC14B. HEK293T cells were transfected with *MeCP2-FLAG*. MeCP2-FLAG protein was immunoprecipitated using FLAG beads and incubated with recombinant CDC14B-GFP or catalytic inactive CDC14B^{C314S}-GFP in vitro. The MeCP2^{pS92}/MeCP2 ratio was densitometrically measured and is depicted in the graph next to the immunoblot. The quantification was performed on three independent experiments. IP, immunoprecipitation. (E to G) Results are means ± SD. Two-tailed unpaired *t* test. n.s. (not significant) $P > 0.05$, $^{**}P < 0.01$, and $^{****}P < 0.0001$.

Biotin-Protein Ligase(BirA)-Human Influenza Hemagglutinin(HA) as bait (fig. S1, A to C, and table S2).

Mass spectrometry analysis identified ser^{92} of MeCP2 [MeCP2^{pS92}; corresponds to ser^{80} of MeCP2 isoform e2 (*20*)] as hypophosphorylated residue in cells expressing Tet$_{ON}$-*CDC14B-YFP* (table S1). Because ScCDC14 activity is linked to mitosis and CDC14B chromatin binding is strongly enhanced in mitosis (*12*, *19*), we next tested whether MeCP2^{pS92} is a substrate of CDC14B during the mitotic phase. Immunoblotting with phospho-specific antibodies revealed accumulation of MeCP2^{pS92} in NOC-arrested nontransformed human telomerase reverse transcriptase immortalized retinal pigment epithelial cells (hTERT RPE1) , which was twofold stronger in *CDC14B*$^{-/-}$ cells compared to wild-type (WT) RPE1 cells but not seen in *CDC14A*$^{-/-}$ cells indicating that MeCP2^{pS92} is a substrate of CDC14B in mitosis (Fig. 1E and fig. S2A; MeCP2^{pS92} antibody specificity was confirmed using MeCP2^{pS92}-FLAG mutants in fig. S2B). In addition, expression of *CDC14B* but not the phosphatase dead *CDC14B*^{C314S} dephosphorylated MeCP2^{pS92} in vivo (Fig. 1F) and the immunoprecipitated MeCP2^{pS92} was directly dephosphorylated by purified CDC14B in vitro (Fig. 1G). Thus, MeCP2^{pS92} is a CDC14B substrate.

MeCP2 is hyperphosphorylated by HIPK2 kinase in cells with prolonged mitosis

To better understand the condition under which MeCP2^{pS92} is phosphorylated, we incubated RPE1 cells with cell cycle–interfering drugs and monitored MeCP2^{pS92} phosphorylation (Fig. 2A). Adriamycin (ADR), an inhibitor of topoisomerase II that increase DNA damage (*21*) and stops cell cycle progression of RPE1 cells in G_1-S and G_2, therefore depleting mitotic cells from the culture (fig. S2, C to E), did only mildly trigger MeCP2^{pS92} phosphorylation even when the treatment was for 24 hours (Fig. 2A and fig. S2, F and G). In contrast, NOC that blocked the cell cycle of cells in prometaphase (fig. S2E) strongly promoted MeCP2^{pS92} accumulation (Fig. 2A and fig. S2, F and G). This suggests that either SAC activation by NOC or the general arrest in mitosis and not DNA damage or G_2 arrest predominantly promotes phosphorylation of MeCP2 at ser^{92}.

HIPK2 kinase has the ability to phosphorylate MeCP2 at ser^{92} (*22*). We observed that the normally unstable HIPK2 (*23*) accumulated in ADR- and NOC-arrested cells and that HIPK2 depletion had a strong impact on MeCP2^{pS92} phosphorylation in NOC-arrested cells (Fig. 2, A to C). Twenty-four hours after drug treatment, the accumulation of HIPK2 was pronounced in NOC-arrested cells compared to the ADR-treated cells (fig. S2, F and H). Furthermore, HIPK2 showed an electrophoretic mobility upshift in response to mitotic arrest that was not observed in ADR-treated cells (Fig. 2A and fig. S2F). Incubation of cell lysates with lambda phosphatase revoked the reduced HIPK2 electrophoretic mobility providing strong evidence that HIPK2 is phosphorylated upon NOC treatment (Fig. 2D).

We next tested the impact on HIPK2 and MeCP2^{S92} phosphorylation in cells synchronously entering mitosis with or without addition of NOC, paclitaxel, or the proteasome inhibitor Carbobenzoxy-Leu-Leu-Leucinal (MG132) (synchronization scheme in Fig. 2E, top). These drugs arrest cells in prometaphase/metaphase and activate the SAC to various degree, with MG132 being the weakest activator as indicated by low BubR1 association with kinetochores (Fig. 2, F and G). HIPK2 was phosphorylated under all mitotic arrest conditions as indicated by the electrophoretic upshift of the HIPK2 band (Fig. 2E, lanes 4 to 10). This upshift was more pronounced when cells were incubated for longer times with NOC, paclitaxel, and inhibitor MG132 (Fig. 2E, compare lanes 5 to 7 with lanes 8 to 10), indicating that the time in mitosis fosters accumulation of MeCP2^{pS92}. Phosphorylation of MeCP2^{pS92} was detected under all prolonged mitotic arrest conditions even when SAC activity was low (MG132) and also occurred to some degree in mitotic cells without perturbations demonstrating that MeCP2^{pS92} phosphorylation by HIPK2 is not triggered by the SAC per se (Fig. 2E). To test whether the mitotic HIPK2 phosphorylation was dependent on SAC activity, we added the inhibitor reversine that targets the key SAC kinase Monopolar Spindle 1 (MPS1) (*24*). As expected, reversine induced rapid mitotic slippage in NOC or paclitaxel-treated cells indicated by a decrease of the mitosis marker histone H3^{pS10}, a collapse of the HIPK2 protein band upshift and diminished phosphorylation of MeCP2^{pS92} (Fig. 2E, lanes 11 and 12). In contrast, proteasome inhibition by MG132 prevented mitotic exit despite the presence of reversine as suggested by persistent high H3^{pS10} signal (Fig. 2E, lane 13). In addition, BubR1 kinetochore localization was low in MG132/reversine-treated cells, suggesting that these cells were arrested in metaphase with little SAC activity (Fig. 2, F and G). HIPK2 upshift and hyperphosphorylation of MeCP2^{pS92} were still observed in these MG132/reversine cells, indicating that prolonged mitosis and not a SAC kinase affects HIPK2 (Fig. 2E, lane 13). Thus, HIPK2 is up-regulated in mitosis to act on MeCP2^{pS92}.

CDC14B and HIPK2 regulate mitotic arrest duration

Upon *CDC14B* overexpression in RPE1 cells arrested in prometaphase by NOC, we observed a decrease of the mitosis marker histone H3^{pS10} (Fig. 1F) and an early emergence of cells that slipped through the mitotic arrest (fig. S3, A and B). Therefore, we used live-cell imaging to measure mitotic arrest duration dependent on *CDC14B*. Genetic ablation of *CDC14B* [*CDC14B* knockout (KO)] but not *CDC14A* KO increased mitotic arrest duration from approximately 30 hours, as observed in WT cells, to 36 hours (Fig. 3, A and B, and fig. S3C). This was apparent with a range of NOC concentrations (0.33 to 3.3 μM), the microtubule stabilizer paxlitaxel and the Eg5 inhibitor STLC (fig. S3, C to F). Furthermore, we were able to rescue the *CDC14B* KO phenotype by expressing the WT *CDC14B-mSc* but not by expressing the phosphatase dead mutant *CDC14B*^{C314S}*-mSc* (Fig. 3C). In addition, overexpressed *CDC14B-mSc*, but not *CDC14B*^{C314S}*-mSc*, decreased the mitotic arrest duration of RPE1 WT cells (Fig. 3D). Together, these data indicate that the arrest duration in response to mitotic challenges is critically dependent on CDC14B activity.

To test the function of MeCP2 in determining the duration of mitotic arrest, we depleted MeCP2 by small interfering RNA (siRNA) (fig. S3G) and measured duration of mitosis by live-cell imaging (Fig. 3E). MeCP2 depletion rescued the prolonged mitotic arrest in *CDC14B* KO cells (Fig. 3E). MeCP2 depletion in RPE1 WT cells also reduced the time of mitotic arrest in response to NOC (Fig. 3E). MeCP2-depleted RPE1 WT and *CDC14B* KO cells showed comparable mitotic arrest duration, indicating that MeCP2 functions downstream of CDC14B (Fig. 3E).

Next, we overexpressed *MeCP2*, the phospho-inhibitory *MeCP2*^{S92A} and the phospho-mimetic *MeCP2*^{S92E} versions in RPE1 WT Tet$_{ON}$ cells to verify the impact of this MeCP2

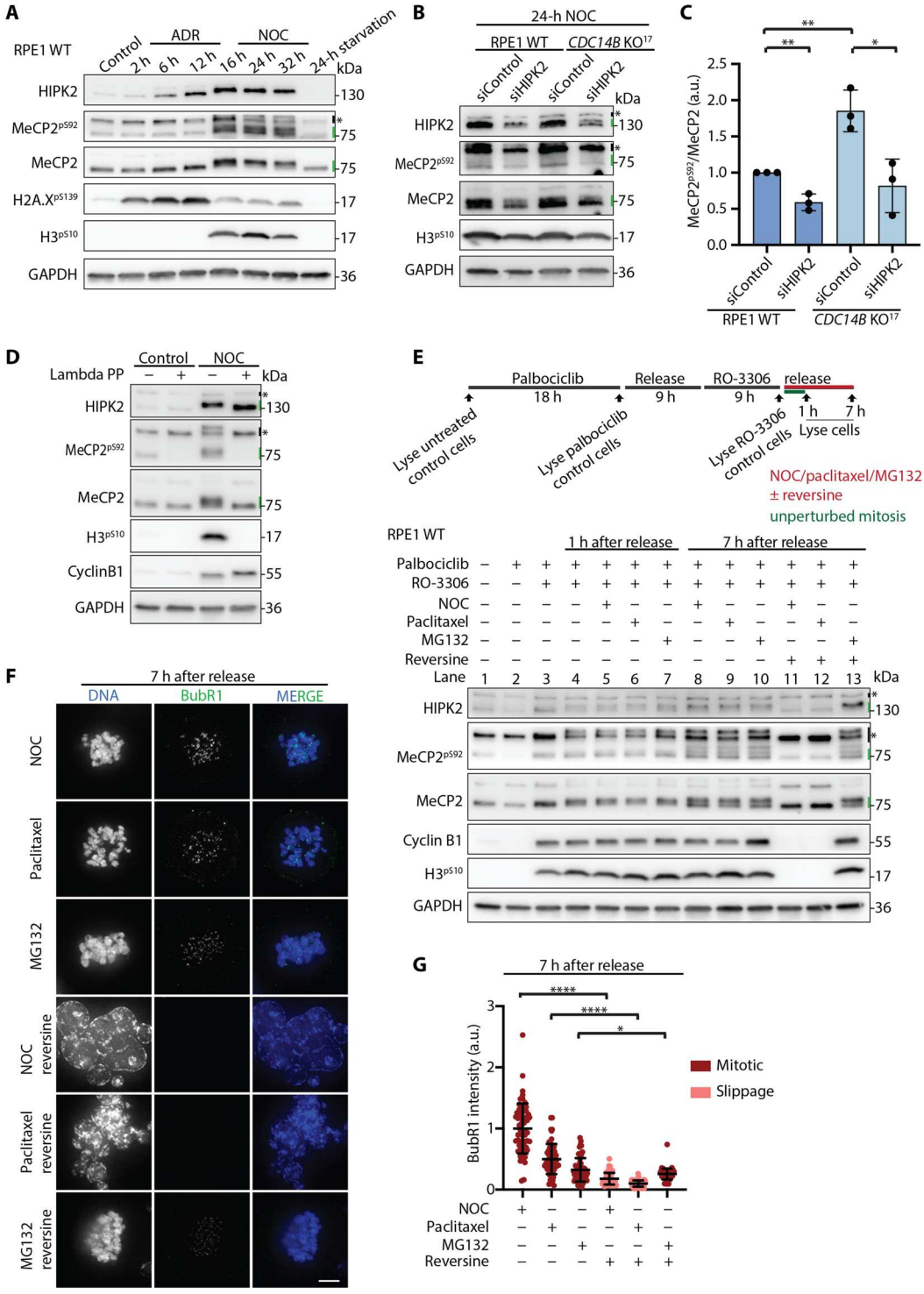

Fig. 2. MeCP2 is phosphorylated by HIPK2. (**A**) RPE1 WT cells were treated with 1.5 μM ADR, 3.3 μM NOC, or serum-free medium, and immunoblot samples were analyzed for MeCP2^{pS92} and HIPK2. The asterisk/black line indicates nonspecific protein bands. Green lines depict position of specific bands. (**B**) RPE1 WT and *CDC14B* KO cells were first treated with siControl or siHIPK2 and subsequently challenged with 3.3 μM NOC. Immunoblot reveals the phosphorylation status of MeCP2 upon HIPK2 depletion. Asterisk and lines as in (A). (**C**) Ratio of densitometrically measured MeCP2^{pS92}/MeCP2 signal from (B). The quantification was performed on three independent experiments. (**D**) Cell lysate derived from NOC (3.3 μM)–treated RPE1 WT cells was incubated with lambda phosphatase. Asterisk and lines as in (A). (**E**) RPE1 WT cells were treated with palbociclib followed by RO-3306, as indicated to enable synchronous entry into mitosis in the presence of 3.3 μM NOC, 0.5 μM paclitaxel, or 10 μM MG132. Reversine (1 μM) was added to abrogate the SAC. Asterisk and lines as in (A). (**F**) Representative immunofluorescence (IF) images for BubR1 of cells from (E). Scale bar, 5 μm. (**G**) Quantification of BubR1 signal intensity of cells from (F) to judge SAC strength. $n = 60$ cells in each group from three independent experiments. (C and G) Results are means ± SD. Two-tailed unpaired *t* test. $^{*}P < 0.05$, $^{**}P < 0.01$, and $^{****}P < 0.0001$.

phospho-site on mitotic duration. Similar mitotic arrest durations were observed between the Tet control cells and cells overexpressing MeCP2^{S92A}. However, overexpressed MeCP2^{WT} and MeCP2^{S92E} (fig. S2B) prolonged the time of mitotic arrest (Fig. 3F), suggesting that the MeCP2^{pS92} counteracts mitotic slippage of cells. If this is the case, then depletion of HIPK2, the kinase that phosphorylates MeCP2, should decrease the mitotic arrest duration in RPE1 WT cells and relieve the phenotype in *CDC14B* KO cells. This was the case (Fig. 3G). In addition, overexpression of the phospho-mimetic *MeCP2^{S92E}* in *CDC14B* KO cells counteracted the effect of HIPK2 depletion, demonstrating that phosphoregulation of MeCP2^{pS92} by HIPK2 and CDC14B regulates mitotic arrest duration (Fig. 3H).

We next asked whether HIPK2-MeCP2 axis is also important in cells with relative weak mitotic disturbances. For this, we turned to

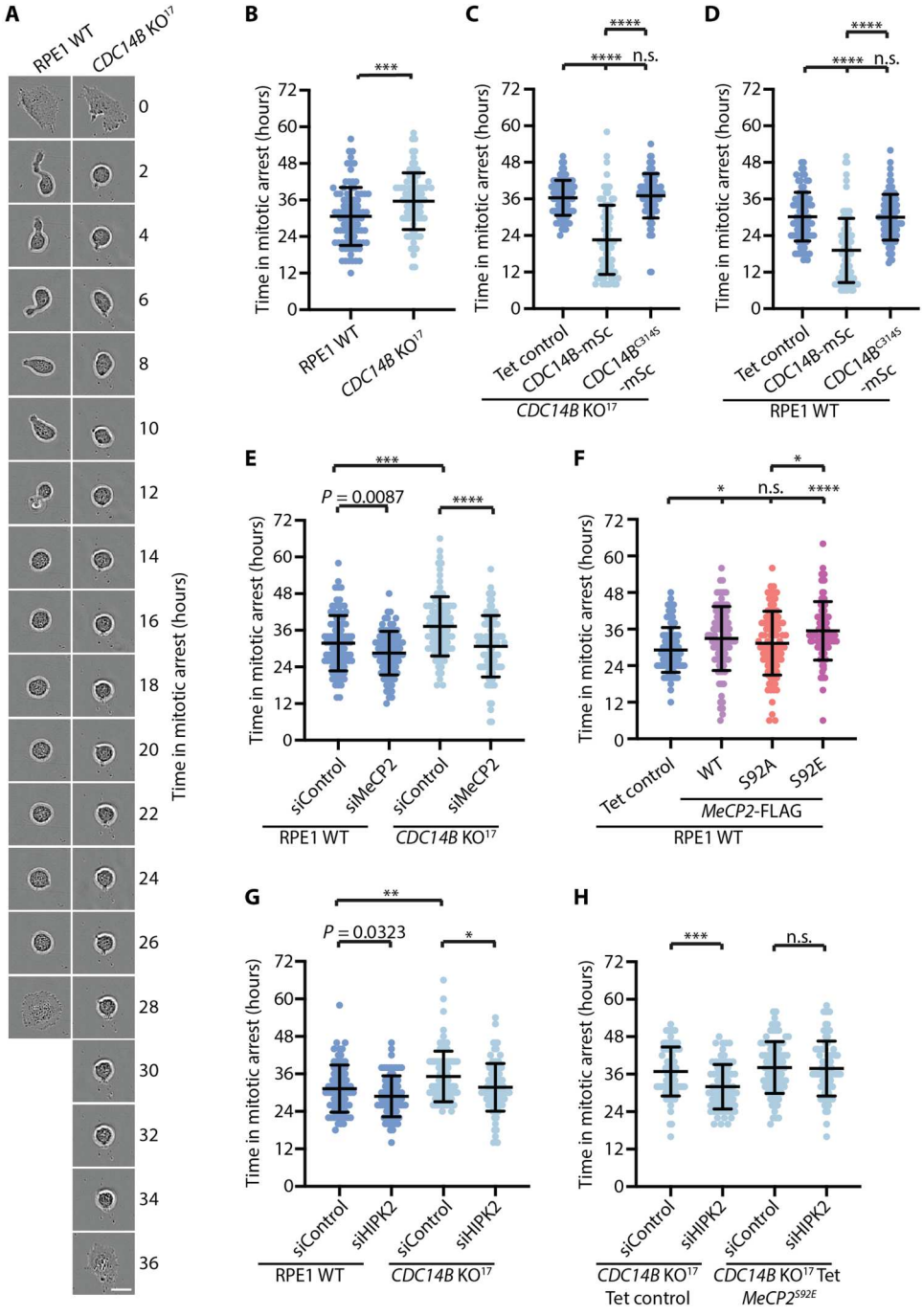

Fig. 3. Mitotic arrest duration is prolonged in *CDC14B* KO cells. (**A**) Live-cell images of NOC-arrested (3.3 μM) RPE1 WT and *CDC14B* KO cells. Elapsed time between mitotic entry (cell rounding) and the loss of the spherical shape was determined. Scale bar, 20 μm. (**B** to **H**) Mitotic arrest duration was assessed as outlined in (A) RPE1 WT and *CDC14B* KO cells (B); *CDC14B* KO Tet_{ON} *CDC14B-mSc* and Tet_{ON} *CDC14B*^{C314S}*-mSc* cells (C); RPE1 WT Tet_{ON} *CDC14B-mSc* and Tet_{ON} *CDC14B*^{C314S}*-mSc* cells (D); MeCP2-depleted RPE1 WT and *CDC14B* KO cells (E); RPE1 WT Tet_{ON} *MeCP2*^{WT}, Tet_{ON} *MeCP2*^{S92A}, and Tet_{ON} *MeCP2*^{S92E} cells (F); HIPK2-depleted RPE1 WT and *CDC14B* KO cells (G); and HIPK2-depleted *CDC14B* KO Tet_{ON} *MeCP2*^{S92E} cells (H). (B) Two-tailed unpaired *t* test. (C, D, F, and H) One-way analysis of variance (ANOVA). (E and G) Two-tailed unpaired *t* test (pairwise comparison written as *P* value). One-way ANOVA (global comparison indicated with stars). (B) *n* = 91 (WT) and 83 (*CDC14B* KO) cells from three independent experiments. (C to F) *n* = 90 cells in each group from three independent experiments. (G) *n* = 80, 77, 82, and 87 cells (from left to right) from three independent experiments. (H) *n* = 86, 76, 91, and 82 (from left to right) cells from three independent experiments. (B to H) Results are means ± SD. n.s. $P > 0.05$, $^{*}P < 0.05$, $^{**}P < 0.01$, $^{***}P < 0.001$, and $^{****}P < 0.0001$.

Δ*N-GCP6* cells that have a mild defect in the microtubule nucleator, the γ-tubulin ring complex (*25*). Δ*N-GCP6* cells showed prolongation of mitosis by 5 min due to weak microtubule defects that delay SAC inactivation. HIPK2 depletion did not affect the mitotic delay in Δ*N-GCP6* cells (fig. S3, H and I). This suggests that the HIPK2-CDC14B-MeCP2^{pS92} axis constitutes a mechanism only important for severe mitotic defects.

CDK1-cyclin B1 activity determines length of the SAC block

Cyclin B1 plays an important role in mitotic arrest duration, and its degradation overrides an active SAC (*6*). CDC14B somehow regulates cyclin B1 because *CDC14B* KO MEF cells increased transcription of several cell cycle regulators including cyclin B1 (*26*). It was suggested that hyperphosphorylation of C-terminal domain (CTD)–ser^5 of the RNA polymerase II (Pol II) mediates enhanced transcription (*26*). We confirmed hyperphosphorylation of Pol II CTD-ser^5 in *CDC14B* KO and *CDC14A* KO cells using a phospho-specific antibody (fig. S4, A and B). However, *CDC14B* KO cells but not *CDC14A* KO cells showed substantially more mitotic cyclin B1 on the protein (Fig. 4A) and transcriptional level (Fig. 4B, left graph) compared to WT suggesting that CDC14B controls cyclin B1 by other mechanisms than Pol II CTD-ser5 hyperphosphorylation.

We next addressed whether MeCP2 phospho-regulation affects cyclin B1 levels. Depletion of MeCP2 reduced mitotic cyclin B1 protein levels in *CDC14B* KO cells to levels comparable to WT cells (Fig. 4, C and D). In addition, overexpression of *MeCP2* and the phospho-mimetic *MeCP2^{S92E}*, but not the phospho-inhibitory *MeCP2^{S92A}*, increased mitotic cyclin B1 amounts (Fig. 4E). Unexpectedly, cyclin B1 transcript levels were not affected by overexpression of *MeCP2*, *MeCP2^{S92A}*, or *MeCP2^{S92E}* (Fig. 4B, right graph). Thus, CDC14B regulates cyclin B1 by a posttranscriptional mechanism through MeCP2.

To verify the hypothesis that increased CDK1-cyclin B1 activity is the cause of elevated mitotic arrest duration in *CDC14B* KO cells, we examined the dose-dependent response of prometaphase arrested RPE1 WT and *CDC14B* KO cells toward the CDK1-cyclin B1 inhibitor RO-3306. The addition of 20 μM RO-3306 promoted nearly immediate mitotic exit in NOC-arrested RPE1 *CDC14B* KO cells that was indistinguishable from WT cells. However, at 10 and 5 μM RO-3306, *CDC14B* KO cells exited mitosis later compared to WT cells, consistent with a higher CDK1–cyclin B1 activity in *CDC14B*-deleted cells that block mitotic exit (Fig. 4F). Furthermore, prometaphase-arrested *CDC14B* KO cells showed pronounced phosphorylation of CDK substrates compared to the WT control confirming a more resilient CDK1–cyclin B1 activity in prometaphase-arrested *CDC14B* KO cells consistent with the increase in cyclin B1 levels in these cells (fig. S4, C to E).

It is believed that prominent CDK1–cyclin B1 activity promotes cell death in mitosis because it delays mitotic slippage and thus provides more time for death signals to accumulate (*27*, *28*). Compared to WT cells, the cell fate profile of *CDC14B* KO cells shifted from slippage toward mitotic cell death, similar to that of WT cells overexpressing *CCNB1* (cyclin B1 gene; Fig. 4G and fig. S5, A to D). The arrest duration of RPE1 WT cells that underwent mitotic slippage or mitotic cell death was indistinguishable, and both arrest times were increased to the same extent in RPE1 *CDC14B* KO cells and in WT cells overexpressing *CCNB1* (Fig. 4H and fig. S5E). The probability of dying after slippage in the subsequent interphase was unaltered among the cell lines (fig. S5, F and G).

Together, MeCP2^{pS92} posttranscriptionally increases mitotic cyclin B1 levels, thereby elevating the CDK1–cyclin B1 activity in cells with abolished CDC14B activity. Enhanced CDK1–cyclin B1 activity prolongs mitotic arrest duration. Despite the delay of slippage out of mitosis caused by hyperactive CDK1, eventually, more cells died in mitosis.

Translation efficiency of cyclin B1 is enhanced by MeCP2^{pS92}

How could CDC14B post transcriptionally control cyclin B1 protein levels? The SAC via the mitotic checkpoint complex (MCC) could be up-regulated in *CDC14B* KO cells, leading to a more efficient blockage of APC/C molecules and deaccelerated cyclin B1 ubiquitination and degradation. However, NOC-arrested RPE1 WT and *CDC14B* KO cells did not show differences in the kinetochore localization of the MCC component BubR1 or in the ability to degrade overexpressed cyclin B1–mCherry (fig. S6, A to C) excluding this possibility.

To judge cyclin B1 turnover during prolonged mitosis, we treated NOC-arrested RPE1 WT and *CDC14B*-deleted cells with the translation inhibitor cycloheximide (CHX) or the proteasome inhibitor MG132 for 3 hours. We detected that 20% of cyclin B1 was degraded in both RPE1 WT and *CDC14B* KO cells after 3 hours of translation inhibition by CHX (Fig. 5, A and B). Conversely, inhibition of the proteasomal degradation machinery by MG132 for 3 hours led to a slight increase of cyclin B1 protein levels, which was more pronounced in the absence of *CDC14B* (Fig. 5, A and B). This indicates that protein synthesis is more pronounced in *CDC14B* KO cells compared to WT. Consistently, double inhibition of protein synthesis and proteasome activity kept cyclin B1 levels in both cell types constant (Fig. 5, A and B). This result emphasizes the importance of mitotic cyclin B1 translation to sustain the SAC block (*29*).

We asked whether CDC14B controls the translation of cyclin B1 through MeCP2^{pS92}. Therefore, we used a live-cell fluorescence reporter that allows accurate measurement of individual protein translation rates (*30*). In brief, the reporter expresses a degron coupled to superfolding variant of GFP (sfGFP) flanked by the untranslated regions (UTRs) from cyclin B1 (*CCNB1*). sfGFP is constantly degraded until addition of the small-molecule stabilizer trimethoprim (TMP). From the same transcript, mCherry is translated separately for normalization of copy number. We found that translation of the reporter bearing control UTRs was strongly repressed in prometaphase-arrested cells and that the *CCNB1*-derived UTRs had a stimulating effect on translation (Fig. 5, C to E). *CDC14B* KO cells showed similar repression of translation with the control reporter, whereas the enhancement of translation rate induced by the *CCNB1* UTRs was more pronounced compared to WT cells (Fig. 5, D and E). In addition, depletion of HIPK2 negatively affected the cyclin B1 translation efficiency in prometaphase-arrested RPE1 WT and *CDC14B* KO cells (fig. S6D). Notably, MeCP2^{WT} and MeCP2^{S92E}, but not MeCP2^{S92A} expressing cells, displayed increased translation efficiency of the *CCNB1* reporter compared to the Tet control cells (Fig. 5F). The MeCP2-mediated effect on cyclin B1 translation was also seen using the translation reporter bearing only the 5′UTR of *CCNB1*, whereas the 3′UTR on its own was dispensable for the translational enhancement

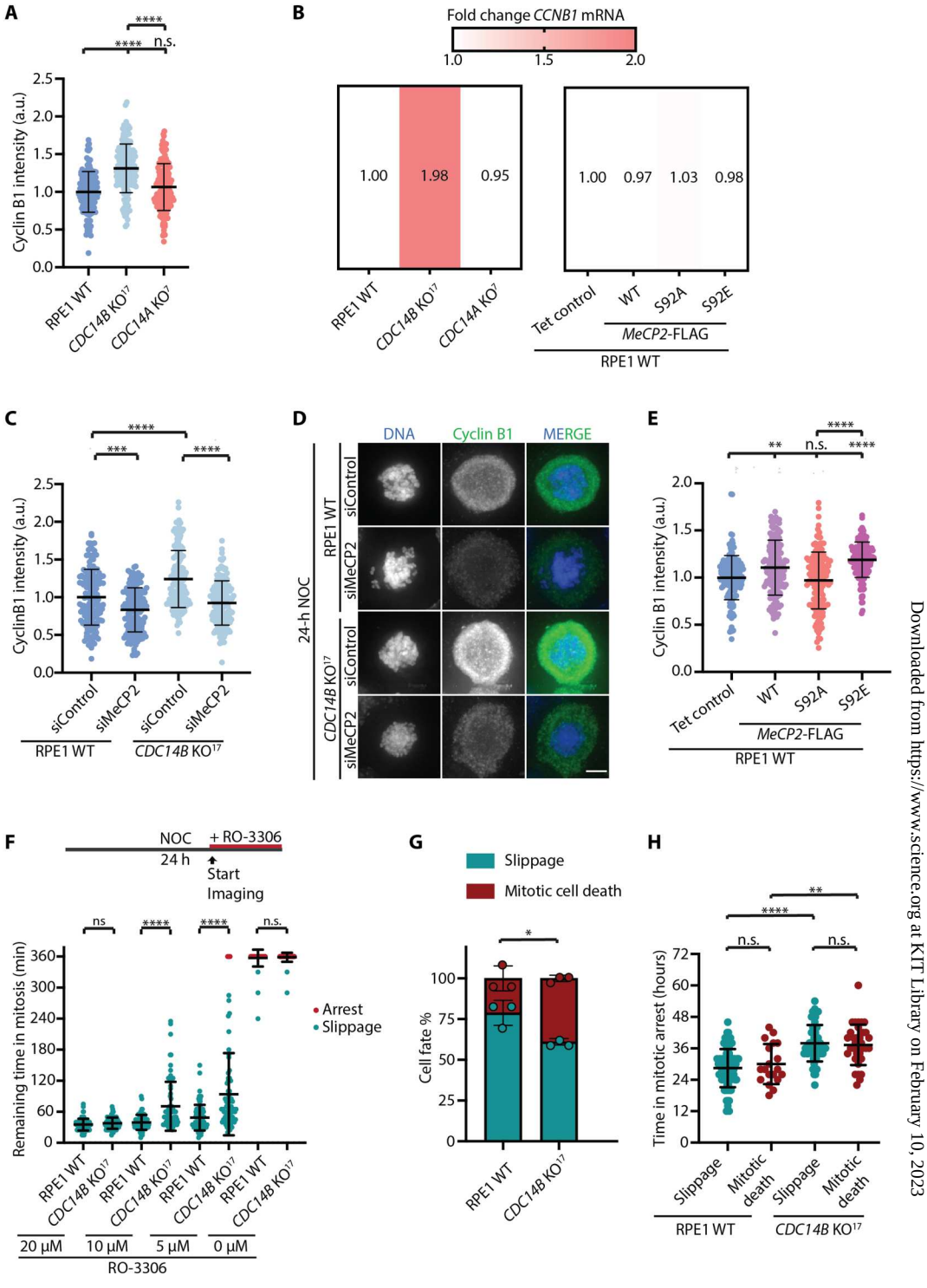

Fig. 4. Elevated cyclin B1 protein levels sustain the SAC. (**A**) RPE1 WT, *CDC14B* KO, and *CDC14A* KO cells were treated with 3.3 μM NOC for 24 hours before fixation, and mitotic cyclin B1 protein levels were analyzed by IF microscopy. $n = 150$ cells in each group from two independent experiments. (**B**) Cyclin B1 transcript level of indicated cell lines treated with 3.3 μM NOC. Heatmap depicts mean value of three technical replicates. (**C**) MeCP2-depleted RPE1 WT and *CDC14B* KO cells were treated and analyzed as in (A). $n = 150$ cells in each group from two independent experiments. (**D**) Representative IF images of (C). Scale bar, 5 μm. (**E**) RPE1 WT Tet_{ON} $MeCP2^{WT}$, Tet_{ON} $MeCP2^{S92A}$, and Tet_{ON} $MeCP2^{S92E}$ were treated and analyzed as in (A). $n = 150$ cells in each group from three independent experiments. (**F**) Prometaphase-arrested RPE1 WT and *CDC14B* KO cells were treated with CDK1 inhibitor RO-3306 at indicated concentrations, and live-cell images were collected at 5-min intervals. $n = 75$ cells in each group from three independent experiments. (**G** and **H**) Mitotic cell fate analysis (G) and arrest duration (H) of NOC (3.3 μM)–treated RPE1 WT and *CDC14B* KO cells. $n = 90$ cells per cell line from three independent experiments. (A, C, and E) One-way ANOVA. (F, G, and H) Two-tailed unpaired *t* test. (A, C, E, and F to H) Results are means ± SD. n.s. $P > 0.05$, $^{**}P < 0.01$, $^{***}P < 0.001$, and $^{****}P < 0.0001$.

(fig. S6, E to H). This finding suggests that the 5′UTR of *CCNB1* is sufficient to promote MeCP2-dependent translation of *CCNB1* in mitosis.

DISCUSSION

The SAC surveys kinetochore attachment to the spindle and delays anaphase onset until all kinetochores have achieved biorientation (*31*). In the event of an irresolvable spindle defect, as caused by some chemotherapeutic agents, cells die in mitosis or alternatively escape cell death by mitotic slippage, a process that is believed to limit effectiveness of anticancer drugs (*3*). Mitotic slippage is

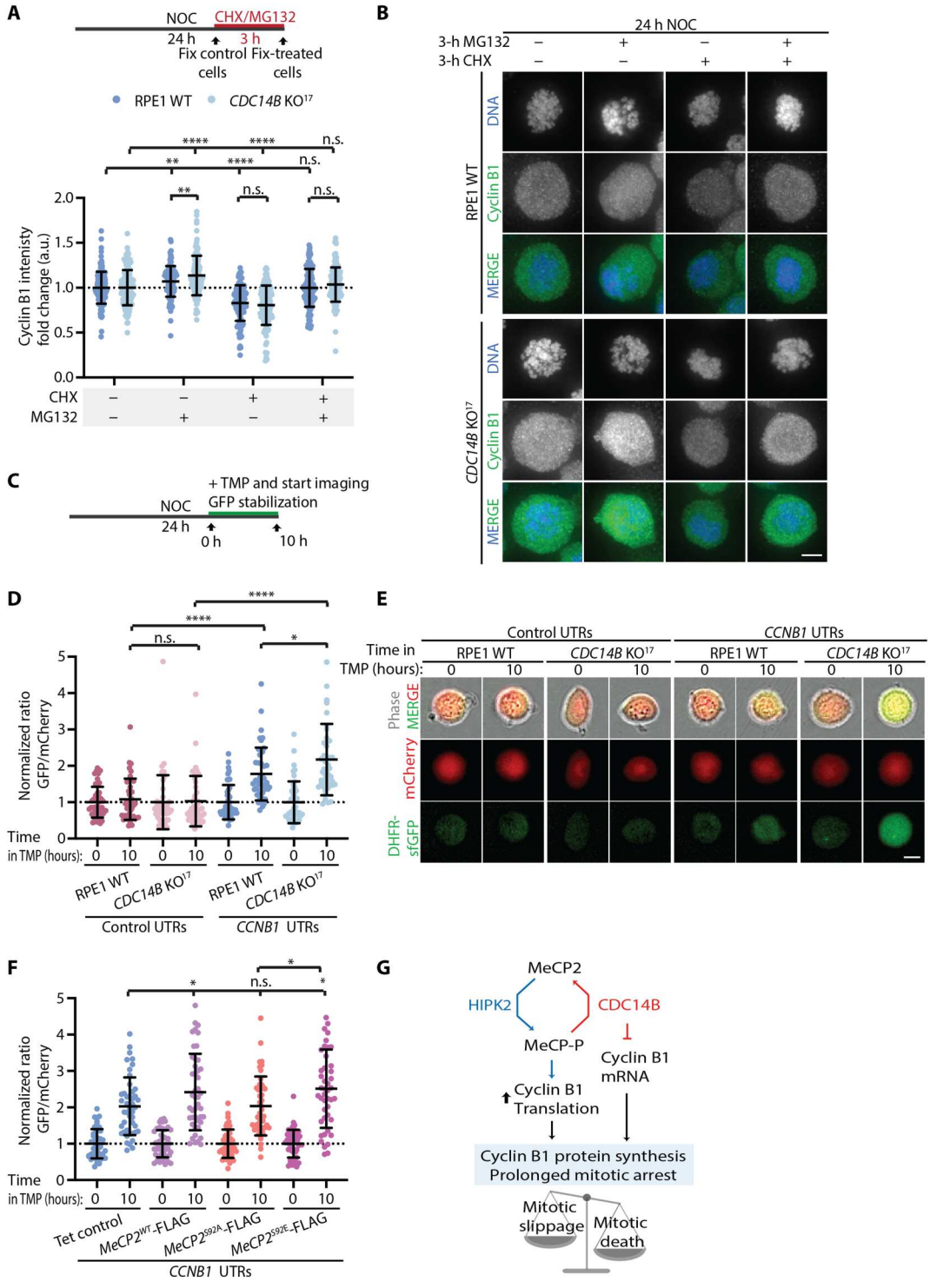

Fig. 5. Translation efficiency of cyclin B1 is enhanced by MeCP2^{pS92}. (**A**) NOC-arrested (3.3 μM) RPE1 WT and *CDC14B* KO cells were monitored for cyclin B1 levels 0 and 3 hours after addition of MG132 and CHX, respectively. Relative change of cyclin B1 intensity between the respective untreated control sample and 3-hour–treated sample was assessed. n = 139, 133, 121, 128, 127, 129, 130, and 128 cells (from left to right) from two independent experiments. (**B**) Representative IF images from (A). Scale bar, 5 μm. (**C**) Experimental scheme for translation measurements. Prometaphase-arrested RPE1 cells expressing a fluorescence-based translation reporter were treated with the stabilizer TMP followed by live-cell imaging. (**D**) 5′UTR and 3′UTR of *CCNB1* were inserted into a fluorescence translation reporter. RPE1 WT and *CDC14B* KO cells stably expressing a control or the *CCNB1* reporter were treated as described in (C) to determine translation efficiency in prometaphase arrest. n = 45 cells in each group from three independent experiments. (**E**) Representative live-cell images from (D). Scale bar, 10 μm. (**F**) RPE1 Tet$_{ON}$ *MeCP2^{WT}*, *MeCP2^{S92A}*, and *MeCP2^{S92E}* cell lines expressing the *CCNB1* translation reporter were treated as described in (C). n = 45 cells in each group from three independent experiments. (**G**) Proposed model summarizing the effect of the HIPK2/CDC14B-MeCP2 axis on mitotic arrest duration. (A, D, and F) Results are means ± SD. Two-tailed unpaired t test. n.s. $P > 0.05$, *$P < 0.05$, **$P < 0.01$, and ****$P < 0.0001$.

concerning because cells become polyploidy and genetically unstable, which may contribute to cell transformation. The prevailing view is that gradual decline of cyclin B1 triggers mitotic slippage (*6*). Declining SAC activity, leakiness of the SAC-induced APC/C block (*32*), or alternative E3 ligases that function parallel to APC/C (*33*) have been considered as causes for the cyclin B1 decline. Because the translation machinery is largely shut down during mitosis (*34*), the contribution of cyclin B1 synthesis for the control of mitotic arrest has been neglected. However, cyclin B1 mRNA is unusual because it is translated in mitosis (*29*). Here, we show that, during mitotic arrest, MeCP2 becomes progressively phosphorylated by HIPK2 counteracted by CDC14B (Fig. 5G). MeCP2^{pS92} then promotes mitotic translation of cyclin B1, leading to an increase in CDK1-cyclin B1 activity that retains cells

with active SAC in mitosis. In addition, prolonged mitotic arrest induced by high cyclin B1 has an impact on cell fate decision because it favors mitotic cell death over slippage into G_1. Thus, mitotic translation of cyclin B1 mRNA regulated by the HIPK2/CDC14B-MeCP2 axis is a decisive but yet unappreciated decision maker of cell fate and cell cycle control in cells with mitotic damages.

MeCP2 is well known for its role in transcriptional regulation (*35*–*37*). The action of MeCP2 on cyclin B1 mRNA translation is exiting and expands the spectrum of MeCP2's functions. How MeCP2 regulates cyclin B1 mRNA is still unclear but our data suggest that the 5′UTR of *CCNB1* is important for the MeCP2-dependent translation in mitosis. The 5′UTR of *CCNB1* might contain a noncanonical internal ribosome entry site (*38*, *39*). Polyadenylation elongation relieving cap-dependent translation inhibition (*40*) as is the case for stored cyclin B1 mRNA during oocyte maturation and nonembryonic mitosis (*41*) is less likely because the 3′UTR of *CCNB1* had no impact on the translation reporter.

MATERIALS AND METHODS

Cell culture and treatments

RPE1, human embryonic kidney (HEK) 293T, and HEK293-GP (GP2-293, Clontech) cells were cultured in Gibco Dulbecco's Modified Eagle's medium (DMEM)/F-12 (Thermo Fisher Scientific) medium supplemented with 10% fetal bovine serum (FBS), 1% L-glutamine, and 1% penicillin/streptomycin. All cell lines were cultured at 37°C and 5% CO_2. RNA interference transfection was carried out according to the manufacturer's protocol (Thermo Fisher Scientific). The following siRNA oligos were purchased from Dharmacon and used at a final concentration of 20 nM: control siRNA (D-001810-10), MeCP2 siRNA (J-013094-07-0005), and HIPK2 siRNA (5′-AAGCGUCGGGUGAAUAUGUA U-3′). To arrest cells in prometahase, if not otherwise stated, 3.3 μM NOC (Sigma-Aldrich), 0.5 μM paclitaxel (Sigma-Aldrich), or 5 μM STLC (Sigma-Aldrich) was used. To arrest cells at G_2-M, cells were first arrested in G_1 using 0.1 μM palbociclib (Tocris) for 18 hours, and 9 hours after palbociclib washout, 10 μM RO-3306 (Sigma-Aldrich) was added for 9 hours. To block cells in metaphase and to inhibit proteasome activity, MG132 (Selleck Chemicals) was used at 10 μM. To abrogate the SAC, the MPS1 inhibitor reversine (Selleck Chemicals) was used at 1 μM. CHX (3.5 μM; Sigma-Aldrich) was used to inhibit protein translation. ADR (Sigma-Aldrich) was used at 1.5 μM. To induce mitotic slippage, CDK1 inhibitor RO-3306 (Sigma-Aldrich) was used at 5, 10, or 20 μM. Protein expression in RPE1 Tet_{ON} cell lines was induced by adding doxycicline (5 ng/ml; Sigma-Aldrich).

Generation of KO and stable cell lines

Zinc finger nuclease–generated RPE1 *CDC14B* KO and *CDC14A* KO cell lines were described previously (*14*, *42*). MeCP2 (NM_001110792) complementary DNA was purchased from Genescript (OHu28304D). RPE1 cells stably expressing the translational reporter and inducible Tet_{ON} cell lines were constructed as described previously (*30*, *43*).

Phospho-proteome and BioID mass spectrometry

Global phospho-proteome and BioID analysis was conducted as previously described (*17*). For phospho-proteome analysis, HeLa Tet_{ON} cell lines were cultured in light ($Arg^{12}C^{14}N$ $Lys^{12}C^{14}N$) and heavy ($Arg^{13}C^{15}Lys^{13}C^{15}N$) stable isotope labeling by/with amino acids in cell culture (SILAC) medium (Silantes) for eight passages before inducing *CDC14B-YFP* and *YFP* expression for 24 hours, respectively. Protein extracts were mixed 1:1, and phospho-peptides were enriched by strong cation exchange chromatography (SCX)/immobilized metal affinity chromatography (IMAC) before LC-MS/MS analysis. For BioID mass spectrometry analysis, expression of CDC14B-BirA and BirA was induced in the presence of 50 nM biotin for 24 hours, respectively, and biotinylated proteins were enriched using streptavidin Sepharose beads (GE Life Sciences) at 4°C for 1 hour. Peptides were identified by MaxQuant software and analyzed using Perseus.

Flow cytometry

Cells were washed once with phosphate-buffered saline (PBS) and fixed with 70% ethanol in PBS at −20°C for 3 hours before permeabilization with 0.25% Triton X-100 in PBS for 15 min on ice. Fixed and permeabilized cells were stained with anti-$H3^{pS10}$ (Cell Signaling Technology, 3377; 1:1000; rabbit) overnight at 4°C. After washing with PBS containing 1% bovine serum albumin (BSA), cells were stained with Alexa Fluor 488–labeled secondary antibody (Invitrogen, A-21206; 1:500) for 30 min at room temperature. Washed cells were incubated with ribonuclease A (100 μg/ml) in the dark at 37°C for 30 min. Propidium iodide staining solution (25 μg/ml) was added shortly before cells were subjected for cell cytometry analysis (BD FACSCanto).

Immunoblotting

Harvested cells were lysed with Laemmli buffer supplemented with protease inhibitor (Roche, 11873580001), phosphatase inhibitor (Roche, 04906845001), phenylmethylsulfonyl fluoride, and benzonase (Merck, 101656). Lysate was heated at 95°C for 5 min, clarified by centrifugation at 20,000*g* for 5 min, and subjected to SDS–polyacrylamide gel electrophoresis (SDS-PAGE). Separated proteins were transferred onto a 0.2-μm polyvinylidene difluoride membrane in 7 min using the Trans-Blot Turbo Transfer System (Bio-Rad) according to the manufacturer's protocol. Proteins were probed with the following antibodies at indicated dilutions: MeCP2 (Cell Signaling Technology, 3456; 1:1000), $MeCP2^{pS80/92}$ (Thermo Fisher Scientific, PA5-104679; 1:2000), $H3^{pS10}$ (Cell Signaling Technology, 3377; 1:1000), $H2A.X^{pS139}$ (Cell Signaling Technology, 9718; 1:1000), HIPK2 [a gift from T. Hofmann; (*23*)], cyclin B1 (Cell Signaling Technology, 4135S; 1:2000), RNA Pol II CTD ^{pS5} (active motif, AB_2793198; 1:2000), phospho-CDK substrate motif (Cell Signaling Technology, 9477; 1:1000), FLAG (Proteintech, 20543-1-AP; 1:5000), GFP (Roche, 11814460 001; 1:1000), and glyceraldehyde-3-phosphate dehydrogenase (GAPDH) (Cell Signaling Technology, 2118; 1:2000). Appropriate peroxidase horseradish peroxidase–conjugated antibodies were purchased from Jackson ImmunoResearch and diluted 1:10,000 (305-035-045 and 715-035-151).

IF microscopy

For indirect immunofluorescence (IF) microscopy, cells were grown on coverslips, treated as indicated, and fixed with either methanol for 5 min at −20°C or paraformaldehyde for 10 min at room temperature. Fixed cells were permeabilized using 0.1% Triton X-100 for 10 min at room temperature. After 1-hour blocking with 10%

FBS in PBS, cells were incubated with primary antibodies followed by appropriate secondary antibody (Invitrogen, 1:500) and Hoechst (1:2000) diluted in 3% BSA in PBS for 1 hour at room temperature, respectively. Coverslips were mounted on glass slides using Moviol, and images were acquired using a DeltaVision RT system (Applied Precision) with an Olympus IX71 microscope equipped with 60× and 100× objective lenses. The following antibodies were used: BubR1 (Abcam, ab4637; 1:100; methanol fixation), $H3^{pS10}$ (Cell Signaling Technology, 3377; 1:800; methanol fixation), cyclin B1 (Cell Signaling Technology, 4138; 1:200; paraformaldehyde fixation), and Cenp-F (a gift from S. Taylor; 1:1000; methanol fixation). Appropriate secondary Alexa Fluor 488–, Alexa Fluor 555–, and Alexa Fluor 647–coupled antibodies were purchased from Invitrogen and diluted at 1:500.

Live-cell imaging

Cells were cultured in DMEM/F-12 complete medium without phenol red (Thermo Fisher Scientific) and treated as indicated. Live-cell images were acquired using the incubator-based Incucyte S3 imager system (Sartorius) equipped with 10× and 20× objective lenses. If not otherwise indicated, images were acquired every 2 hours for 72 hours. Mitotic arrest duration and subsequent cell fate were judged by morphological hallmarks as previously described (*44*). Cell growth (confluency) was monitored and quantified using the Incucyte automated live-cell analysis system according to the manufacturer's protocol.

Fluorescence-based translation reporter

The live-cell fluorescence-based translation reporter system was developed in RPE1 cells elsewhere (Addgene, plasmid no. 67929). *CCNB1* 5′UTR and 3′UTR were polymerase chain reaction (PCR)–amplified from RPE1 genomic DNA and inserted into the translation reporter vector as previously described (*30*). The reporter translates an unstable dihydrofolate reductase–sfGFP protein, which is stabilized upon the addition of TMP. A 2A self-cleaving peptide (P2A) ribosome-skipping site allows separate expression of a stable mCherry protein from the same transcript used for copy number normalization. The increase of GFP/mCherry ratio over time upon TPM addition reports the translation efficiency. Prometaphase-arrested RPE1 cells stably expressing the reporter were treated with 50 μM TMP and subjected to live-cell imaging. Increase of GFP/mCherry ratio was analyzed using Image J software.

Quantitative reverse transcription polymerase chain reaction

Total RNA was extracted from cells using TRIsure (Bioline, catalog no. BIO-38033) according to the manufacturer's protocol. One microgram of isolated RNA was reverse-transcribed using the QuantiTect Reverse Transcriptase Kit (Qiagen, catalog no. 205311). Quantitative PCR was performed on QuantStudio3 (Applied Biosystems) using an SYBR green master mix (Applied Biosystems, catalog no. 4364344). GAPDH was used as reference gene, and all primer sequences used were previously published (*45*, *46*): CCNB1, 5′-TTCTGGATAATGGTGAATGGAC-3′ (forward) and 5′-ATGT GGCATACTTGTTCTTGAC-3′ (reverse); and GAPDH, 5′-CCAC TCCTCCACCTTTGAC-3′ (forward) and 5′-ACCCTGTTGCTGT AGCCA-3′ (reverse).

In vitro phosphatase assay

Protein extract from RPE1 cells for in vitro dephosphorylation assay was obtained using ice-cold radioimmunoprecipitation assay (RIPA) buffer supplemented with protease inhibitor (Roche, 11873580001), phenylmethylsulfonyl fluoride, and benzonase (Merck, 101656). Lambda phosphatase and assay buffer were added according to the manufacturer's protocol (New England Biolabs, no. P0753). Treated and buffer control samples were incubated at 30°C for 30 min. Samples were spiked with Laemmli buffer, heated at 95°C for 5 min, and subjected to SDS-PAGE followed by immunoblot to analyze products.

In vitro dephosphorylation assay

MeCP2-FLAG construct was transfected into HEK293T cells using polyethylenimine. Cells were lysed with ice-cold RIPA buffer supplemented with protease inhibitor (Roche, 11873580001), phenylmethylsulfonyl fluoride, and benzonase (Merck, 101656). Forty-eight hours after transfection, MeCP2-FLAG was immunoprecipitated using FLAG magnetic beads (Sigma-Aldrich, M8823) according to the manufacturer's protocol. Eluted MeCP2-FLAG was coincubated with purified CDC14B or phosphatase dead $CDC14B^{C314S}$ in phosphatase assay buffer (30 mM imidazole, 1 mM dithiothreitol, 1 mM EDTA, 150 mM KCl, 1 mM $MgCl_2$, and 25 mM K-Hepes) for 2 hours at 30°C. To determine the extent of dephosphorylation, samples were subjected to SDS-PAGE followed by immunoblot, and $MeCP2^{pS92}$/MeCP2 ratio was densitometrically quantified.

Supplementary Materials

This PDF file includes:
Figs. S1 to S6

Other Supplementary Material for this manuscript includes the following:
Tables S1 and S2

View/request a protocol for this paper from *Bio-protocol*.

REFERENCES AND NOTES

1. M. McGill, B. R. Brinkley, Mitosis in human leukemic leukocytes during colcemid inhibition and recovery. *Cancer Res.* **32**, 746–755 (1972).
2. V. Sudakin, D. Ganoth, A. Dahan, H. Heller, J. Hershko, F. C. Luca, J. V. Ruderman, A. Hershko, The cyclosome, a large complex containing cyclin-selective ubiquitin ligase activity, targets cyclins for destruction at the end of mitosis. *Mol. Biol. Cell* **6**, 185–197 (1995).
3. R. S. Balachandran, E. T. Kipreos, Addressing a weakness of anticancer therapy with mitosis inhibitors: Mitotic slippage. *Mol. Cell. Oncol.* **4**, e1277293 (2017).
4. L. M. Zasadil, K. A. Andersen, D. Yeum, G. B. Rocque, L. G. Wilke, A. J. Tevaarwerk, R. T. Raines, M. E. Burkard, B. A. Weaver, Cytotoxicity of paclitaxel in breast cancer ts due to chromosome missegregation on multipolar spindles. *Sci. Transl. Med.* **6**, 229ra43 (2014).
5. T. Fujiwara, M. Bandi, M. Nitta, E. V. Ivanova, R. T. Bronson, D. Pellman, Cytokinesis failure generating tetraploids promotes tumorigenesis in p53-null cells. *Nature* **437**, 1043–1047 (2005).
6. D. A. Brito, C. L. Rieder, Mitotic checkpoint slippage in humans occurs via cyclin B destruction in the presence of an active checkpoint. *Curr. Biol.* **16**, 1194–1200 (2006).
7. R. Visintin, K. Craig, E. S. Hwang, S. Prinz, M. Tyers, A. Amon, The phosphatase Cdc14 triggers mitotic exit by reversal of Cdk-dependent phosphorylation. *Mol. Cell* **2**, 709–718 (1998).
8. S. L. Jaspersen, J. F. Charles, D. O. Morgan, Inhibitory phosphorylation of the APC regulator Hct1 is controlled by the kinase Cdc28 and the phosphatase Cdc14. *Curr. Biol.* **9**, 227–236 (1999).

9. S. Palani, F. Meitinger, M. E. Boehm, W. D. Lehmann, G. Pereira, Cdc14-dependent dephosphorylation of Inn1 contributes to Inn1-Cyk3 complex formation. *J. Cell Sci.* **125**, 3091–3096 (2012).
10. E. Raspelli, C. Cassani, E. Chiroli, R. Fraschini, Budding yeast Swe1 is involved in the control of mitotic spindle elongation and is regulated by Cdc14 phosphatase during mitosis. *J. Biol. Chem.* **290**, 1–12 (2015).
11. J. Holder, E. Poser, F. A. Barr, Getting out of mitosis: Spatial and temporal control of mitotic exit and cytokinesis by PP1 and PP2A. *FEBS Lett.* **593**, 2908–2924 (2019).
12. E. Berdougo, M. V. Nachury, P. K. Jackson, P. V. Jallepalli, The nucleolar phosphatase Cdc14B is dispensable for chromosome segregation and mitotic exit in human cells. *Cell Cycle* **7**, 1184–1190 (2008).
13. P. Partscht, B. Uddin, E. Schiebel, Human cells lacking CDC14A and CDC14B show differences in ciliogenesis but not in mitotic progression. *J. Cell Sci.* **134**, jcs255950 (2021).
14. N.-P. Chen, B. Uddin, R. Voit, E. Schiebel, Human phosphatase CDC14A is recruited to the cell leading edge to regulate cell migration and adhesion. *Proc. Natl. Acad. Sci. U.S.A.* **113**, 990–995 (2016).
15. B. Uddin, P. Partscht, N.-P. Chen, A. Neuner, M. Weiß, R. Hardt, A. Jafarpour, B. Heßling, T. Ruppert, H. Lorenz, G. Pereira, E. Schiebel, The human phosphatase CDC14A modulates primary cilium length by regulating centrosomal actin nucleation. *EMBO Rep.* **20**, e46544 (2019).
16. R. E. Amir, I. B. van den Veyver, M. Wan, C. Q. Tran, U. Francke, H. Y. Zoghbi, Rett syndrome is caused by mutations in X-linked MECP2, encoding methyl-CpG-binding protein 2. *Nat. Genet.* **23**, 185–188 (1999).
17. N.-P. Chen, B. Uddin, R. Hardt, W. Ding, M. Panic, I. Lucibello, P. Kammerer, T. Ruppert, E. Schiebel, Human phosphatase CDC14A regulates actin organization through dephosphorylation of epithelial protein lost in neoplasm. *Proc. Natl. Acad. Sci. U.S.A.* **114**, 5201–5206 (2017).
18. C. L. Eissler, G. Mazón, B. L. Powers, S. N. Savinov, L. S. Symington, M. C. Hall, The Cdk/cDc14 module controls activation of the Yen1 holliday junction resolvase to promote genome stability. *Mol. Cell* **54**, 80–93 (2014).
19. A. Mocciaro, E. Schiebel, Cdc14: A highly conserved family of phosphatases with non-conserved functions? *J. Cell Sci.* **123**, 2867–2876 (2010).
20. S. Kriaucionis, A. Bird, The major form of MeCP2 has a novel N-terminus generated by alternative splicing. *Nucleic Acids Res.* **32**, 1818–1823 (2004).
21. W. Y. Siu, T. Arooz, R. Y. Poon, Differential responses of proliferating versus quiescent cells to adriamycin. *Exp. Cell Res.* **250**, 131–141 (1999).
22. G. Bracaglia, B. Conca, A. Bergo, L. Rusconi, Z. Zhou, M. E. Greenberg, N. Landsberger, S. Soddu, C. Kilstrup-Nielsen, Methyl-CpG-binding protein 2 is phosphorylated by homeodomain-interacting protein kinase 2 and contributes to apoptosis. *EMBO Rep.* **10**, 1327–1333 (2009).
23. M. Winter, D. Sombroek, I. Dauth, J. Moehlenbrink, K. Scheuermann, J. Crone, T. G. Hofmann, Control of HIPK2 stability by ubiquitin ligase Siah-1 and checkpoint kinases ATM and ATR. *Nat. Cell Biol.* **10**, 812–824 (2008).
24. S. Santaguida, A. Tighe, A. M. D'Alise, S. S. Taylor, A. Musacchio, Dissecting the role of MPS1 in chromosome biorientation and the spindle checkpoint through the small molecule inhibitor reversine. *J. Cell Biol.* **190**, 73–87 (2010).
25. M. Würtz, E. Zupa, E. S. Atorino, A. Neuner, A. Böhler, A. S. Rahadian, B. J. A. Vermeulen, G. Tonon, S. Eustermann, E. Schiebel, S. Pfeffer, Modular assembly of the principal microtubule nucleator γ-TuRC. *Nat. Commun.* **13**, 473 (2022).
26. M. Guillamot, E. Manchado, M. Chiesa, G. Gómez-López, D. G. Pisano, M. P. Sacristán, M. Malumbres, Cdc14b regulates mammalian RNA polymerase II and represses cell cycle transcription. *Sci. Rep.* **1**, 189 (2011).
27. M. E. Bekier, R. Fischbach, J. Lee, W. R. Taylor, Length of mitotic arrest induced by microtubule-stabilizing drugs determines cell death after mitotic exit. *Mol. Cancer Ther.* **8**, 1646–1654 (2009).
28. A. Ghelli Luserna di Rorà, G. Martinelli, G. Simonetti, The balance between mitotic death and mitotic slippage in acute leukemia: A new therapeutic window? *J. Hematol. Oncol.* **12**, 123 (2019).
29. S. Sciortino, A. Gurtner, I. Manni, G. Fontemaggi, A. Dey, A. Sacchi, K. Ozato, G. Piaggio, The cyclin B1 gene is actively transcribed during mitosis in HeLa cells. *EMBO Rep.* **2**, 1018–1023 (2001).
30. M. E. Tanenbaum, N. Stern-Ginossar, J. S. Weissman, R. D. Vale, Regulation of mRNA translation during mitosis. *eLife* **4**, e07957 (2015).
31. R. E. Zirkle, Ultraviolet-microbeam irradiation of newt-cell cytoplasm: Spindle destruction, false anaphase, and delay of true anaphase. *Radiat. Res.* **41**, 516–537 (1970).
32. T. M. Lok, Y. Wang, W. K. Xu, S. Xie, H. T. Ma, R. Y. C. Poon, Mitotic slippage is determined by p31comet and the weakening of the spindle-assembly checkpoint. *Oncogene* **39**, 2819–2834 (2020).
33. R. S. Balachandran, C. S. Heighington, N. G. Starostina, J. W. Anderson, D. L. Owen, S. Vasudevan, E. T. Kipreos, The ubiquitin ligase CRL2ZYG11 targets cyclin B1 for degradation in a conserved pathway that facilitates mitotic slippage. *J. Cell Biol.* **215**, 151–166 (2016).
34. H. Fan, S. Penman, Regulation of protein synthesis in mammalian cells. *J. Mol. Biol.* **50**, 655–670 (1970).
35. X. Nan, H. H. Ng, C. A. Johnson, C. D. Laherty, B. M. Turner, R. N. Eisenman, A. Bird, Transcriptional repression by the methyl-CpG-binding protein MeCP2 involves a histone deacetylase complex. *Nature* **393**, 386–389 (1998).
36. M. Chahrour, S. Y. Jung, C. Shaw, X. Zhou, S. T. C. Wong, J. Qin, H. Y. Zoghbi, MeCP2, a key contributor to neurological disease, activates and represses transcription. *Science* **320**, 1224–1229 (2008).
37. L. D. Boxer, W. Renthal, A. W. Greben, T. Whitwam, A. Silberfeld, H. Stroud, E. Li, M. G. Yang, B. Kinde, E. C. Griffith, B. Bonev, M. E. Greenberg, MeCP2 represses the rate of transcriptional initiation of highly methylated long genes. *Mol. Cell* **77**, 294–309.e9 (2020).
38. S. An, O. S. Kwon, J. Yu, S. K. Jang, A cyclin-dependent kinase, CDK11/p58, represses cap-dependent translation during mitosis. *Cell. Mol. Life Sci.* **77**, 4693–4708 (2020).
39. L. Marash, N. Liberman, S. Henis-Korenblit, G. Sivan, E. Reem, O. Elroy-Stein, A. Kimchi, DAP5 promotes cap-independent translation of Bcl-2 and CDK1 to facilitate cell survival during mitosis. *Mol. Cell* **30**, 447–459 (2008).
40. R. Mendez, J. D. Richter, Translational control by CPEB: A means to the end. *Nat. Rev. Mol. Cell Biol.* **2**, 521–529 (2001).
41. I. Novoa, J. Gallego, P. G. Ferreira, R. Mendez, Mitotic cell-cycle progression is regulated by CPEB1 and CPEB4-dependent translational control. *Nat. Cell Biol.* **12**, 447–456 (2010).
42. B. Uddin, N.-P. Chen, M. Panic, E. Schiebel, Genome editing through large insertion leads to the skipping of targeted exon. *BMC Genomics* **16**, 1082 (2015).
43. R. Vlijm, X. Li, M. Panic, D. Rüthnick, S. Hata, F. Herrmannsdörfer, T. Kuner, M. Heilemann, J. Engelhardt, S. W. Hell, E. Schiebel, STED nanoscopy of the centrosome linker reveals a CEP68-organized, periodic rootletin network anchored to a C-Nap1 ring at centrioles. *Proc. Natl. Acad. Sci. U.S.A.* **115**, E2246–E2253 (2018).
44. D. A. Brito, C. L. Rieder, The ability to survive mitosis in the presence of microtubule poisons differs significantly between human nontransformed (RPE-1) and cancer (U2OS, HeLa) cells. *Cell Motil. Cytoskeleton* **66**, 437–447 (2009).
45. P. Mlcochova, H. Winstone, L. Zuliani-Alvarez, R. K. Gupta, TLR4-mediated pathway triggers interferon-independent G_0 arrest and antiviral SAMHD1 activity in macrophages. *Cell Rep.* **30**, 3972–3980.e5 (2020).
46. R. Contreras-Galindo, S. Fischer, A. K. Saha, J. D. Lundy, P. W. Cervantes, M. Mourad, C. Wang, B. Qian, M. Dai, F. Meng, A. Chinnaiyan, G. S. Omenn, M. H. Kaplan, D. M. Markovitz, Rapid molecular assays to study human centromere genomics. *Genome Res.* **27**, 2040–2049 (2017).

Acknowledgments: We thank M. Langlotz from the ZMBH FACS facility for the cell-sorting experiments and the ZMBH mass spectrometry facility for the analysis of the CDC14B phosphoproteome. We thank T. Hofmann and S. Taylor for sharing the antibodies. **Funding:** This work was supported by the Deutsche Forschungsgemeinschaft grant Schi295/3-4 to E.S. and the European Research Council through the grant ERC-CoG-682496 (cenRNA) to S.E. **Author contributions:** P.P. and E.S. designed the experiments. P.P. performed most of the experiments. A.S. performed the quantitative reverse transcription PCR experiments. P.P. and N.-P.C. performed the SILAC experiments and evaluated the mass spectrometry data. P.P. and E.S. wrote the manuscript. All authors edited and reviewed the manuscript. E.S. and S.E supervised the research. **Competing interests:** The authors declare that they have no competing interests. **Data and materials availability:** All data needed to evaluate the conclusions in the paper are present in the paper and/or the Supplementary Materials.

Submitted 28 June 2022
Accepted 16 December 2022
Published 20 January 2023
10.1126/sciadv.add6982

ScienceAdvances

The HIPK2/CDC14B-MeCP2 axis enhances the spindle assembly checkpoint block by promoting cyclin B translation

Patrick Partscht, Alexander Simon, Nan-Peng Chen, Sylvia Erhardt, and Elmar Schiebel

Sci. Adv., **9** (3), eadd6982.
DOI: 10.1126/sciadv.add6982